*metals*

MDPI

*Article*

# Negative Strain Rate Sensitivity Induced by Structure Heterogeneity in $Zr_{64.13}Cu_{15.75}Ni_{10.12}Al_{10}$ Bulk Metallic Glass

**Xiang Wang, Zhi Qiang Ren, Wei Xiong, Si Nan Liu, Ying Liu, Si Lan and Jing Tao Wang ***

School of Materials Science and Engineering, Nanjing University of Science & Technology, Nanjing 210014, China; xiangwang@njust.edu.cn (X.W.); renzhiqiang@njust.edu.cn (Z.Q.R.); xiongwei1225@njust.edu.cn (W.X.); liusinan@njust.edu.cn (S.N.L.); liuying517@njust.edu.cn (Y.L.); lansi@njust.edu.cn (S.L.)

* Correspondence: jtwang@njust.edu.cn; Tel.: +86-258-4315-493

**Abstract:** The negative strain rate sensitivity (SRS) of metallic glasses is frequently observed. However, the physical essence involved is still not well understood. In the present work, small-angle X-ray scattering (SAXS) and high-resolution transmission electron microscopy (HRTEM) reveal the strong structure heterogeneity at nanometer and tens of nanometer scales, respectively, in bulk metallic glass (BMG) $Zr_{64.13}Cu_{15.75}Ni_{10.12}Al_{10}$ subjected to fully confined compression processing. A transition of SRS of stress, from 0.012 in the as-cast specimen to $-0.005$ in compression processed specimen, was observed through nanoindentation. A qualitative formulation clarifies the critical role of internal stress induced by structural heterogeneity in this transition. It reveals the physical origin of this negative SRS frequently reported in structurally heterogeneous BMG alloys and its composites.

**Keywords:** structural heterogeneity; bulk metallic glass; strain rate sensitivity

check for updates

**Citation:** Wang, X.; Ren, Z.Q.; Xiong, W.; Liu, S.N.; Liu, Y.; Lan, S.; Wang, J.T. Negative Strain Rate Sensitivity Induced by Structure Heterogeneity in $Zr_{64.13}Cu_{15.75}Ni_{10.12}Al_{10}$ Bulk Metallic Glass. *Metals* **2021**, *11*, 339. https://doi.org/10.3390/met11020339

Academic Editor: Jordi Sort Viñas

Received: 12 January 2021
Accepted: 11 February 2021
Published: 18 February 2021



## 1. Introduction

The strain rate has a significant effect on the flow stress during the deformation of bulk metallic glasses (BMGs), especially the serrated flow behavior [1–3]. As we all know, a high positive value of strain rate sensitivity (SRS) for conventional crystalline metals represents more homogeneous deformation. However, most of the monolithic BMGs have positive SRS [4–9], a few exhibit negative values [10–12]. It is noteworthy that most of the BMGs exhibiting negative SRS show significant structural heterogeneity. For instance, there is a significant negative SRS in BMGs containing extensive dendrite distribution [13]. Moreover, similar negative SRS has been reported in other MGs containing a composite structure [14–16]. In addition, it has been reported that $Zr_{52.5}Cu_{17.9}Ni_{14.6}Al_{10}Ti_5$ (Vit105) BMG subjected to pre-compression deformation [17] introduced a large number of shear bands, which indicated its structural inhomogeneity increased greatly, so that its SRS changed from positive in the as-cast state to negative after deformation as shown by its strain rate-displacement curve. Thus, this structure heterogeneity will have a significant effect on the mechanical behavior of BMGs. However, how the SRS is affected by the internal structure heterogeneity of the BMGs remains unclear, which requires further investigation.

In this paper, fully confined compression processing was conducted to introduce dense multiple shear bands in monolithic $Zr_{64.13}Cu_{15.75}Ni_{10.12}Al_{10}$ BMG alloy with excellent compression plasticity [18]. These shear bands will serve as interfaces that separate the adjacent and un-sheared amorphous regions, forming a shear band-matrix (loose-dense) heterogeneous structure [19,20] with no phase separation. Nanoindentation of the specimens presented a transition of SRS from a positive value of 0.012 in the as−cast state to a negative value of $-0.005$ after compression processing. The physical mechanism responsible for this SRS transition from positive to negative is explored. A qualitative formulation clarifies the key role of internal stress induced by structural heterogeneity in this transition.

## 2. Materials and Methods

Alloy ingots with a nominal composition $Zr_{64.13}Cu_{15.75}Ni_{10.12}Al_{10}$ were prepared by arc melting from pure elements (purity > 99.9%) in a Ti-gettered argon atmosphere. The ingot was remelted several times for chemical homogeneity and subsequently cast into a water-cooled suction casting machine with a copper mold with a cylindrical cavity of 3 mm diameter. The as-cast BMG rod with a diameter of 3 mm, was cut to a height of ~4.7 mm so that a specimen with an aspect ratio $\geq$1.5 was obtained for compression deformation processing. The compression processing was conducted under full confinement, similar to geometric confinement [21], which produces an equivalent hydrostatic pressure of ~2 GPa in the specimen. This pressure is selected just above the strength of this alloy. The full confinement was maintained during the whole compression deformation process until a compression reduction of ~64%. Then, 5 mm long and 3 mm wide sheet specimens of both as-cast and compressed were obtained using wire cutting and were ground and polished to 30 µm thick for small-angle x-ray scattering (SAXS), using an Anton Parr SAXSpace instrument with a Mo target (wavelength k = 0.0711 nm) to obtain structural information of the specimens. Both as-cast and compressed specimens with a diameter of 3 mm and a thickness of 60 µm were subjected to two-jet electropolishing under nitrogen cooling in a solution of perchloric acid and alcohol (1:9). Then Titan G2 60-300 high-resolution electron microscopy (HRTEM) was used to observe the specimens' microstructural features.

Longitudinal sections of the specimens obtained by wire cutting in the cast state and ~64% compression reduction, respectively, were subjected to nanoindentation experiments on the surface of polished longitudinal sections before and after constrained compression using an ultra-microscopic dynamic hardness tester DUH-211 with a Berkovich diamond indenter. The indentation experiments were conducted at room temperature with a maximum loading force of 200 mN and a dwell time of 5 s. The loading rates were 20 mN/s; 10 mN/s; 2 mN/s; and 1 mN/s, corresponding to strain rates of 0.05 $s^{-1}$; 0.025 $s^{-1}$; 0.005 $s^{-1}$; and 0.0025 $s^{-1}$, respectively, and each strain rate was subjected to at least five indentation tests to ensure the accuracy of strain rate sensitivity (m).

## 3. Results

Figure 1 shows the nanoindentation loading displacement curves for the as-cast and compressed specimens. It can be observed that the apparent serrated flow in the nanoindentation process is suppressed with the strain rate increases, and when a certain critical rate is reached, the serrated flow is completely suppressed and will be unobservable, which is manifested in the loading displacement curve as a shift from a wavy to a smooth curve, especially the compressed samples. This change agrees with the observations reported for various BMGs [22,23] and this is because at a high strain rate, a single shear band is difficult to adapt to rapid deformation, and only multiple shear bands can be activated at the same time, which also leads to the decrease of the width of each serrated flow and disappears at a certain critical strain rate [22]. As shown in Figure 1a, at a low strain rate, the nanoindentation loading displacement curve of the compressed specimen is shifted considerably compared with the as-cast specimen. Meanwhile, in the local amplification of the curve, the as-cast specimen exhibits a wave-like serrated flow, while the compressed specimen's serrated behavior is divided into multiple fine serrated flows with much less serration width. A previous study [2] showed that fine and discrete serrations could diminish shear localization and allow more uniform deformation. In this study, compression introduced a large number of shear bands. This heterogeneous structure formed by compression can coordinate the deformation of BMGs in the nanoindentation. When the strain rate is low, as in Figure 1b, the as-cast specimen still exhibits serrated behavior while the compressed specimen curve is smooth, indicating that the deformation in the nanoindentation activated a large number of existing shear bands of the compressed specimen to achieve uniform deformation [23].

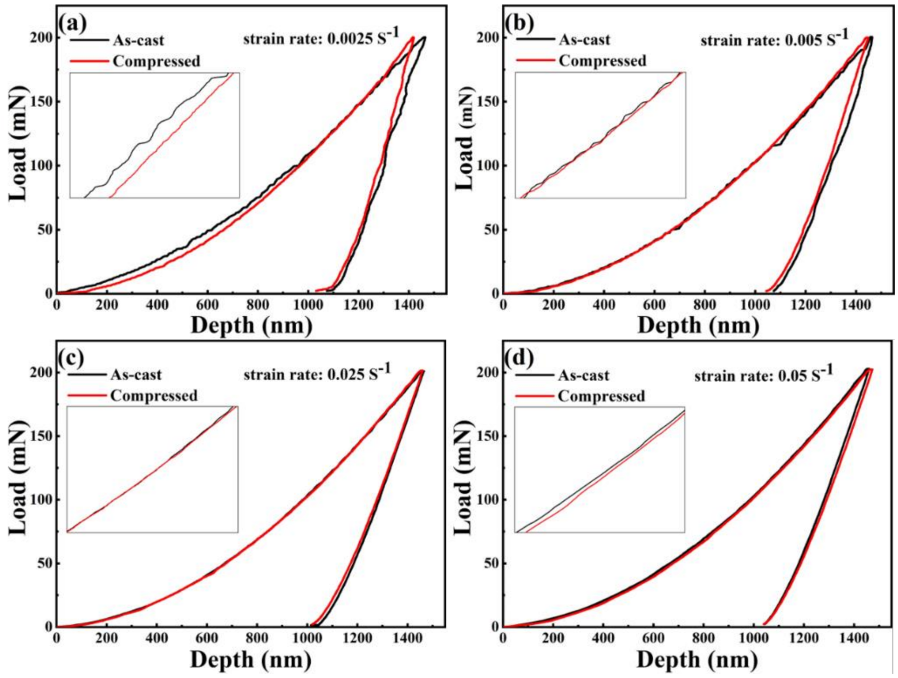


**Figure 1.** Load-penetration curves of as-cast versus compressed BMGs at equivalent strain rates (**a**) 0.0025 $s^{-1}$, (**b**) 0.005 $s^{-1}$, (**c**) 0.025 $s^{-1}$, and (**d**) 0.05 $s^{-1}$.

Figure 2 shows the hardness of as-cast and compressed specimens obtained by nanoindentation at different strain rates. The hardness of the as-cast specimen is significantly lower than the compressed specimen at low strain rates. With the increase of strain rate, the hardness of the as-cast specimen increases, and the hardness of the compressed specimen decreases; and at the highest strain rate in this investigation, the hardness of the as-cast specimen is higher than the compressed specimen. The regression of the hardness-strain rate data yields an SRS value of $0.012 \pm 0.002$ for the as-cast specimen, and $-0.005 \pm 0.002$ for the compressed specimen. The value of SRS of the as-cast sample is similar to those of a previous study [24], but it becomes negative for the compressed specimen. This anomalous result is clearly arising from the structural change during fully confined compression before nanoindentation.

Figure 3 shows the HRTEM results of both as-cast and compressed specimens. No crystallization was observed in either specimen, as evidenced by the insert diffraction patterns. Bright and dark contrast can be observed in the structure, with the bright part predicting a sparser region of atoms. In Figure 3a, the intrinsic local structural inhomogeneity [25] of the as-cast specimen can be seen, although its overall microstructure is homogeneous; and Figure 3b displays its inherent disordered state. After compression, structural inhomogeneity at a scale of tens of nanometers manifested, as can be seen in Figure 3c. Even with further magnification, this high degree of inhomogeneity can still be observed relative to the as-cast specimen, as shown in Figure 3d, where dash lines are added to delineate the boundaries between relatively bright and dark regions, further indicating a dramatic increase in its structural inhomogeneity after fully confined compression deformation. The size of the nanoindentations is 7–8 μm, so the inhomogeneous structure of the compressed specimen will hinder its shear bands propagation during the nanoindentation tests, and thus promote the generation of branching shear bands, as shown by Figure 1a by the smaller serrations of the compressed specimen at the minimum strain rate on the nanoindentation loading displacement curve compared to the as-cast specimen.

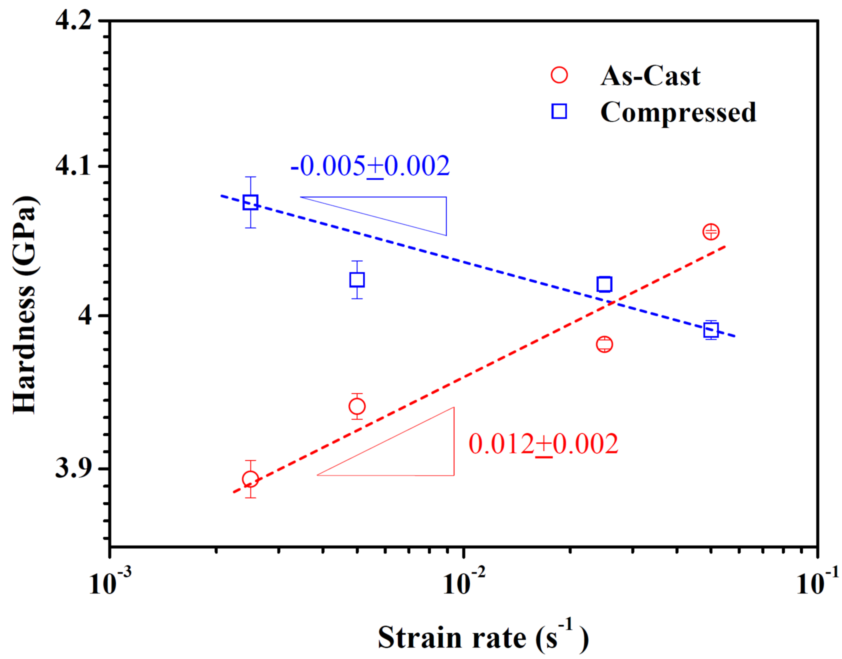


**Figure 2.** Strain rate dependence of hardness from nanoindentations of as-cast and compressed specimens. The slope of the fitted relations (dashed lines) demonstrates the strain rate sensitivity (m).

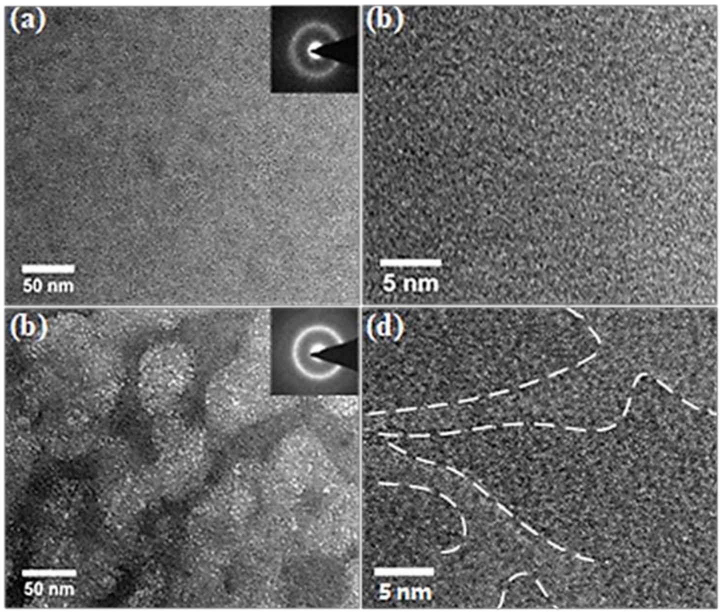


**Figure 3.** HRTEM structure before (**a**,**b**) and after (**c**,**d**) fully confined compression deformation.

Figure 4 shows the SAXS scattering intensity for both as-cast and compressed specimens at the low Q position. Q value variation is related to the scattering angle: $Q = 4\pi \mathrm{Sin}\theta/\lambda$. Here, $\theta$ is half of the scattering angle between the incident and scattered beam. $\lambda$ is the X-ray wavelength. It is clear from the figure that the scattering intensity increases obviously after compression deformation, which indicates enhanced structural inhomogeneity at nanoscale after compression.

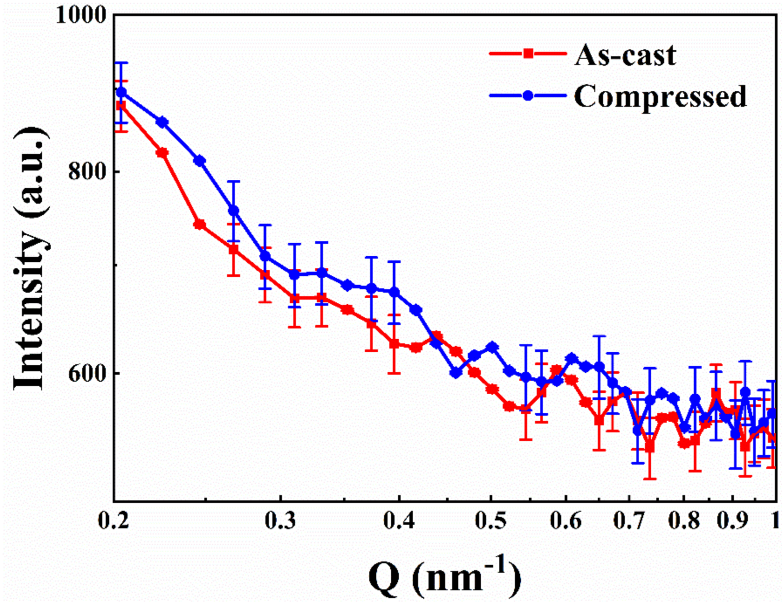


**Figure 4.** SAXS intensity of the as cast and compressed specimens.

## 4. Discussion

Negative SRS is observed in monolithic $Zr_{64.13}Cu_{15.75}Ni_{10.12}Al_{10}$ BMG after the fully confined compression deformation processing in the present study, as shown in Figure 2, together with the heterogeneous structure manifested by SAXS and HRTEM observation, at scales from nano to tens of nanometers, as shown in Figures 3 and 4. This negative SRS is not an isolated incident observation. It has been first reported in $Pd_{80}Si_{20}$ filaments [26], and frequently observed related to heterogeneous structures [27–29] or even composite structures of MGs [12–15]. However, no clear mechanism is proposed to give a persuasive elucidation of the phenomenon, which arises in the following discussions, and finally, a qualitative formula approach is presented to provide the insight links between negative SRS, the feature of BMG structure, and the heterogeneity of the structure.

The negative SRS observed in the Vit105 BMG [30] have been annotated by analogous to the phenomenon of Portevin–Le Châtelier (PLC) deformation bands observed in some crystalline alloys, where dynamic strain aging takes place through the interaction of solute atoms and forest dislocations. However, a detailed investigation indicates that dynamic strain aging-induced solute strengthening of both mobile and forest dislocations is necessitated for the negative SRS that leads to PLC behavior, and solute strengthening of only the mobile dislocation is not enough [31]. It is the solute atom strengthening of the forest dislocations generated during the concurrent deformation process that dominates the negative SRS and PLC behavior. This same mechanism seemed to be difficult since no defects analogous to the forest dislocations in the crystalline alloy is evidenced in monolithic BMG. On the other side, negative SRS is more frequently observed in heterogeneously structured BMG and BMG composites than in uniform, monolithic BMG, which could not be distinguished with the dynamic strain aging mechanism. Thus, alternation other than the dynamic strain aging mechanism is considered.

Observing the deformation behavior of the monolithic BMG in the present investigation, from the viewpoint of flow stress vs. functioning flow defect density (e.g., extending shear band front), one important difference could be recognized in comparison to the crystalline alloys displaying negative strain hardening sensitivity. While the crystalline alloys working in the high defect density region, where strain (defect) hardening dominates, on the deformation mechanism map constructed in the stress-defect density space [32], the monolithic BMG in the present investigation could be analogous to working in the low defect density region, where strain (defect) softening dominates. One obvious argument to support this analogy is that deformation by shear bands in BMG is a nucleation-controlled process [33], and BMGs are usually work softening, and the higher the density of active shear bands, the lower its overall flow stress [34]. This is both phenomenologically and physically the same as that observed in nanocrystalline [35,36] and single crystalline [37] materials. With this basic feature of the monolithic BMG, the negative SRS could be qualitatively formulated.

By analoging the plastic deformation mediated by the "flow defect" of shear band in BMG to the plastic behavior in crystalline materials mediated by the "flow defect" of slip dislocation, the plastic strain rate in BMG could also be expressed by the Orowan equation [38]:

$$\dot{\varepsilon} = \alpha \rho V \tag{1}$$

where, $\rho$ is the density of flow defects; $V$ is the average velocity of flow defects under the action of the stress; and $\alpha$ is a parameter related to the geometry of the flow defects and is independent of flow defects density and velocity.

Considering the definition of strain rate sensitivity $m$:

$$m = \frac{\partial ln\sigma}{\partial ln\dot{\varepsilon}} \tag{2}$$

$$\frac{1}{m} = \frac{\partial ln\dot{\varepsilon}}{\partial ln\sigma} = \frac{\partial ln\rho}{\partial ln\sigma} + \frac{\partial lnV}{\partial ln\sigma} \tag{3}$$

For materials working in the region of low flow defects density on the deformation mechanism map constructed in the stress-defect density space [32], strain (flow defect) softening dominates the deformation, and analogous to the dislocation-mediated plasticity, the relationship between flow stress $\sigma$ and flow defect density $\rho$ could be expressed by equation [39]:

$$\sigma = \frac{\beta}{\rho^n} \tag{4}$$

where, $n > 0$ is the defect density dependence exponent of stress and usually takes the value of 1/2~1; $\beta$ is a coefficient that relates to shear modulus, orientation factor of the flow defects, and the size of the material.

It is clear from Equation (4) that:

$$\frac{\partial ln\rho}{\partial ln\sigma} = -\frac{1}{n} \tag{5}$$

It is a negative item that lays the foundation for a reduced SRS.

Based on the stick-slip shear dynamics and the atomic scale cooperative shearing model of shear transformation zones (STZ), the shear band sliding velocity, $V$, can be expressed as [40]:

$$V = V_0 \exp\left[-\frac{4R\xi G_{0T}\gamma_C^2\Omega}{k_B T}\left(1 - \frac{\sigma}{\sigma_0}\right)^{3/2} + \frac{1}{\chi}\right] \tag{6}$$

where, $V_0$ is the external loading velocity; $k_B$ is the Boltzmann constant; $T$ is the temperature; $G_{0T}$ is the shear modulus at different temperatures; $\gamma_C$ is the critical yield shear strain ($\gamma_C \approx 0.027$); $\Omega$ is the volume of the STZ, R $\approx$ 1/4, $\xi$~2–4; and $\sigma$ and $\sigma_0$ are the yield strengths at temperatures $T$ and 0 K, respectively. $\chi$ is the effective temperature characterizing the state of the configuration disorder and the density or the total number of STZs.

$$\frac{\partial lnV}{\partial ln\sigma} = \frac{6R\xi G_{0T}\gamma_C^2\Omega}{k_B T}\frac{\sigma}{\sigma_0}\left(1 - \frac{\sigma}{\sigma_0}\right)^{1/2} \tag{7}$$

Combine Equations (3), (5) and (7), we obtain:

$$\frac{1}{m} = \frac{\partial ln\dot{\varepsilon}}{\partial ln\sigma} = \frac{\partial ln\rho}{\partial ln\sigma} + \frac{\partial lnV}{\partial ln\sigma} = -\frac{1}{n} + \frac{6R\xi G_{0T}\gamma_C^2\Omega}{k_B T}\frac{\sigma}{\sigma_0}\left(1 - \frac{\sigma}{\sigma_0}\right)^{1/2} \quad (8)$$

In the case of heterogeneous structure, internal stress develops in the BMG matrix, which resists in the sliding of shear band in BMG, and plays a critical role for the transition of SRS from positive to negative. Take the resolved component of such resistance in the direction of the shear band sliding as $\sigma_{\mathrm{i}}$. The effect of external applied stress $\sigma$ would be muffled off by an amount of $\sigma_{\mathrm{i}}$. Thus, a locally effective stress $\sigma_l = \sigma - \sigma_{\mathrm{i}}$, which is the actual resultant stress applied on the shear band front, should be used to replace the external applied stress $\sigma$ in Equation (8), thus:

$$\frac{1}{m} = \frac{\partial ln\dot{\varepsilon}}{\partial ln\sigma} = \frac{\partial ln\rho}{\partial ln\sigma} + \frac{\partial lnV}{\partial ln\sigma} = -\frac{1}{n} + \frac{6R\xi G_{0T}\gamma_C^2\Omega}{k_B T}\frac{\sigma - \sigma_{\mathrm{i}}}{\sigma_0}\left(1 - \frac{\sigma - \sigma_{\mathrm{i}}}{\sigma_0}\right)^{1/2} \quad (9)$$

In Equation (9), the first item on the right, $-\frac{1}{n}$ which is definitely a negative item according to the physical definition of $n$, is the defect density dependence exponent of stress. However, this is not the determinative item for the transition of SRS from positive in the as-cast monolithic BMG to negative in the heterogeneously structured BMG or BMG composites. In the second item to the right of the Equation (9), internal stress $\sigma_{\mathrm{i}}$ arises from the strongly heterogeneous structure that resulted by fully confined compression deformation processing, as observed in the present investigation, or the heterogeneity of composite constituents [13–16]. It is the effect of the internal stress $\sigma_{\mathrm{i}}$ finally that reduces the resultant value of the right items in Equation (9) and transforms from positive to negative, thus resulting in the negative SRS.

## 5. Conclusions

As-cast and compression processed BMG $Zr_{64.13}Cu_{15.75}Ni_{10.12}Al_{10}$ specimens are investigated in the present work, and the structure and property evolution are characterized by HRTEM, SAXS, and nanoindentation. The following conclusions can be drawn from the research:

(1) SAXS and HRTEM reveal the strong structure heterogeneity at nanometer and tens of nanometer scales, respectively, in the Vit105 alloy compression processed to a reduction of ~64%. Compared to the as-cast alloy, these distinctive heterogeneity features stand for the significant potential of modifying BMG structure through proper deformation processing.
(2) A transition of SRS of stress, from 0.012 in the as-cast specimen to −0.005 in the compression-processed specimen, was observed through nanoindentation, accompanied by the gradual vanish of serration phenomenon in the compression processed samples at the increasing strain rate.
(3) Qualitative mathematical formulation, based on the physics of shear band nucleation-controlled plasticity of BMG, describes the inherent link between the observed negative SRS and the internal stress existing in the materials. It reveals the physical origin of this negative SRS frequently reported in structural heterogeneous BMG alloys and its composites.

**Author Contributions:** Conceptualization, J.T.W.; methodology, J.T.W. and X.W.; data curation, X.W., W.X. and S.N.L.; investigation, Y.L. and S.L.; writing—original draft preparation, X.W.; writing—review and editing, J.T.W. and Z.Q.R.; funding acquisition, J.T.W. and S.L. All authors have read and agreed to the published version of the manuscript.

**Funding:** This research was funded by the Natural Science Foundation of China (Grant No. 51520105001, 51871120).

**Conflicts of Interest:** The authors declare no conflict of interest.

## References


1. Burgess, T.; Laws, K.J.; Ferry, M. Effect of loading rate on the serrated flow of a bulk metallic glass during nanoindentation. *Acta Mater.* **2008**, *56*, 4829–4835. [CrossRef]
2. Li, F.C.; Gu, J.; Song, M.; Ni, S.; Guo, S.F. The Evolution of Local Mechanical Properties of Bulk Metallic Glasses Caused by Structural Inhomogeneity. *J. Alloys Compd.* **2014**, *591*, 315–319. [CrossRef]
3. Cheng, L.; Jiao, Z.M.; Ma, S.G.; Qiao, J.W.; Wang, Z.H. Serrated flow behaviors of a Zr-based bulk metallic glass by nanoindentation. *J. Appl. Phys.* **2014**, *115*. [CrossRef]
4. Li, M.C.; Jiang, M.Q.; Jiang, F.; He, L.; Sun, J. Testing effects on hardness of a Zr-based metallic glass under nanoindentation. *Scr. Mater.* **2017**, *138*, 120–123. [CrossRef]
5. Zhao, S.; Wang, H.; Gu, J.; Guo, N.; Shao, L.; Zhang, Y.; Yao, K.; Chen, N. High strain rate sensitivity of hardness in Ti-Zr-Hf-Be-(Cu/Ni) high entropy bulk metallic glasses. *J. Alloys Compd.* **2018**, *742*, 312–317. [CrossRef]
6. Zhou, Q.; Du, Y.; Han, W.; Ren, Y.; Zhai, H.; Wang, H. Identifying the origin of strain rate sensitivity in a high entropy bulk metallic glass. *Scr. Mater.* **2019**, *164*, 121–125. [CrossRef]
7. Ding, Z.Y.; Song, Y.X.; Ma, Y.; Huang, X.W.; Zhang, T.H. Nanoindentation investigation on the size-dependent creep behavior in a Zr-Cu-Ag-Al bulk metallic glass. *Metals.* **2019**, *9*, 613. [CrossRef]
8. Tong, Y.; Qiao, J.C.; Pelletier, J.M.; Yao, Y. Rate-dependent plastic deformation of TiZrHfCuNiBe high entropy bulk metallic glass. *J. Alloys Compd.* **2019**, *785*, 542–552. [CrossRef]
9. Li, M. Effect of annealing on strain rate sensitivity of metallic glass under nanoindentation. *Metals.* **2020**, *10*, 1063. [CrossRef]
10. González, S.; Xie, G.Q.; Louzguine-Luzgin, D.V.; Perepezko, J.H.; Inoue, A. Deformation and Strain Rate Sensitivity of a Zr-Cu-Fe-Al Metallic Glass. *Mat. Sci. Eng. A* **2011**, *528*, 3506–3512. [CrossRef]
11. Dubach, A.; Torre, F.H.D.; Löffler, J.F. Deformation kinetics in Zr-based bulk metallic glasses and its dependence on temperature and strain-rate sensitivity. *Philos. Mag. Lett.* **2007**, *87*, 695–704. [CrossRef]
12. Bhattacharyya, A.; Singh, G.; Eswar-Prasad, K.; Narasimhan, R.; Ramamurty, U. On the strain rate sensitivity of plastic flow in metallic glasses. *Mat. Sci. Eng. A* **2015**, *625*, 245–251. [CrossRef]
13. Tang, Y.L.; Wu, R.F.; Jiao, Z.M.; Shi, X.H.; Wang, Z.H.; Qiao, J.W. Shear softening of Ta-containing metallic glass matrix composites upon dynamic loading. *Mat. Sci. Eng. A* **2017**, *704*, 322–328. [CrossRef]
14. Zhao, J.T.; Zhang, J.Y.; Cao, L.F.; Wang, Y.Q.; Zhang, P.; Wu, K.; Liu, G.; Sun, J. Zr Alloying effect on the microstructure evolution and plastic deformation of nanostructured Cu thin films. *Acta Mater.* **2017**, *132*, 550–564. [CrossRef]
15. Wang, Y.Q.; Zhang, J.Y.; Liang, X.Q.; Wu, K.; Liu, G.; Sun, J. Size- and constituent-dependent deformation mechanisms and strain rate sensitivity in nanolaminated crystalline Cu/amorphous Cu-Zr films. *Acta Mater.* **2015**, *95*, 132–144. [CrossRef]
16. Xue, F.; Huang, P.; Liu, M.B.; Xu, K.W.; Wang, F.; Lu, T.J. Unusual strain rate sensitivity of nanoscale amorphous CuZr/Crystalline Cu multilayers. *Mat. Sci. Eng. A* **2017**, *684*, 84–89. [CrossRef]
17. Jiang, W.H.; Jiang, F.; Liu, F.X.; Wang, Y.D.; Dang, H.M.; Yang, F.Q.; Choo, H.; Liaw, P.K. Mechanical behaviours of workhardening and worksoftening bulk metallic glasses. *Mater. Sci. Technol.* **2012**, *28*, 249–255. [CrossRef]
18. Liu, Y.H.; Wang, G.; Wang, R.J.; Zhao, D.Q.; Pan, M.X.; Wang, W.H. Super Plastic Bulk Metallic Glasses at Room Temperature. *Science* **2007**, *315*, 1385–1388. [CrossRef]
19. Wang, Y.; Li, M.; Xu, J. Toughen and harden metallic glass through designing statistical heterogeneity. *Scr. Mater.* **2016**, *113*, 10–13. [CrossRef]
20. Gleiter, H. Nanoglasses: A new kind of noncrystalline materials. *Beilstein J. Nanotechnol.* **2013**, *4*, 517–533. [CrossRef] [PubMed]
21. Yu, P.; Liu, Y.H.; Wang, G.; Bai, H.Y.; Wang, W.H. Enhance plasticity of bulk metallic glasses by geometric confinement. *J. Mater. Res.* **2007**, *22*, 2384–2388. [CrossRef]
22. Schuh, C.A.; Nieh, T.G. A Nanoindentation Study of Serrated Flow in Bulk Metallic Glasses. *Acta Mater.* **2003**, *51*, 87–99. [CrossRef]
23. Wang, X.L.; Jiang, F.; Hahn, H.; Li, J.; Gleiter, H.; Sun, J.; Fang, J.X. Plasticity of a Scandium-Based Nanoglass. *Scr. Mater.* **2015**, *98*, 40–43. [CrossRef]
24. Pan, D.; Inoue, A.; Sakurai, T.; Chen, M.W. Experimental characterization of shear transformation zones for plastic flow of bulk metallic glasses. *Proc. Natl. Acad. Sci. USA* **2008**, *105*, 14769–14772. [CrossRef]
25. Qiao, J.C.; Wang, Q.; Pelletier, J.M.; Kato, H.; Casalini, R.; Crespo, D.; Pineda, E.; Yao, Y.; Yang, Y. Structural heterogeneities and mechanical behavior of amorphous alloys. *Prog. Mater. Sci.* **2019**, *104*, 250–329. [CrossRef]
26. Maddin, R.; Masumoto, T. The Deformation of Amorphous Palladium-20 at. % Silicon. *Mater. Sci. Eng.* **1972**, *9*, 153–162. [CrossRef]
27. Dubach, A.; Dalla Torre, F.H.; Löffler, J.F. Constitutive model for inhomogeneous flow in bulk metallic glasses. *Acta Mater.* **2009**, *57*, 881–892. [CrossRef]
28. Jiang, W.H.; Liu, F.X.; Jiang, F.; Qiu, K.Q.; Choo, H.; Liaw, P.K. Strain-rate dependence of hardening and softening in compression of a bulk-metallic glass. *J. Mater. Res.* **2007**, *22*, 2655–2658. [CrossRef]
29. Ma, Y.B.; Wang, B.Z.; Zhang, Q.D.; Jiang, Y.; Hou, D.W.; Cui, X.; Zu, F.Q. Change dynamic behaviors by heightening its stored energy of monolithic bulk metallic glass. *Mater. Des.* **2019**, *181*, 107971. [CrossRef]
30. Dalla Torre, F.H.; Dubach, A.; Siegrist, M.E.; Löffler, J.F. Negative strain Rate sensitivity in bulk metallic glass and its similarities with the dynamic Strain aging effect during deformation. *Appl. Phys. Lett.* **2006**, *89*, 8–11. [CrossRef]

31. Soare, M.A.; Curtin, W.A. Solute strengthening of both mobile and forest dislocations: The origin of dynamic strain aging in fcc metals. *Acta Mater.* **2008**, *56*, 4046–4061. [CrossRef]
32. Dieter, G.E. *Mechanical Metallurgy*; McGraw-Hill: New York, NY, USA, 1986. [CrossRef]
33. Perepezko, J.H.; Imhoff, S.D.; Chen, M.W.; Wang, J.Q.; Gonzalez, S. Nucleation of shear bands in amorphous alloys. *Proc. Natl. Acad. Sci. USA* **2014**, *111*, 3938. [CrossRef]
34. Bei, H.; Xie, S.; George, E.P. Softening caused by profuse shear banding in a bulk metallic glass. *Phys. Rev. Lett.* **2006**, *96*, 105503. [CrossRef]
35. Hahn, H.; Mondal, P.; Padmanabhan, K.A. Plastic deformation of nanocrystalline materials. *Nanostruct. Mater.* **1997**, *9*, 603–606. [CrossRef]
36. Schiøtz, J.; Di Tolla, F.D.; Jacobsen, K.W. Softening of nanocrystalline metals at very small grain sizes. *Nature* **1998**, *391*, 561–563. [CrossRef]
37. Maloy, S.A.; Chu, F.; Petrovic, J.J.; Mitchell, T.E. *Dislocations and Mechanical Properties of Single Crystal Niobium Disilicide*; Los Alamos National Lab: Los Alamos, NM, USA, 1996; pp. 1–8. [CrossRef]
38. Orowan, E. Problems of Plastic Gliding. *Proc. Phys. Soc.* **1940**, *52*, 8–22. [CrossRef]
39. El-Awady, J.A. Unravelling the physics of size-dependent dislocation-mediated plasticity. *Nat. Commun.* **2015**, *6*, 1–9. [CrossRef] [PubMed]
40. Bian, X.; Şopu, D.; Wang, G.; Sun, B.; Bednarčik, J.; Gammer, C.; Zhai, Q.; Eckert, J. Signature of local stress states in the deformation behavior of metallic glasses. *NPG Asia Mater.* **2020**. [CrossRef]